Resonant Raman scattering and inner-shell hole widths in Cu, Zn and Ho



1989 J. Phys.: Condens. Matter 1 5955

(http://iopscience.iop.org/0953-8984/1/34/012)

J. Phys.: Condens. Matter 1 (1989) 5955–5964. Printed in the UK

# Resonant Raman scattering and inner-shell hole widths in Cu, Zn and Ho

K Hämäläinen†, S Manninen†, P Suortti†, S P Collins‡, M J Cooper‡ and D Laundy§

† Department of Physics, University of Helsinki, Siltavuorenpenger 20D, SF-00170 Helsinki, Finland

‡ Department of Physics, University of Warwick, Coventry CV4 7AL, UK

§ Daresbury Laboratory, Daresbury, Warrington WA4 4AD, UK

Received 20 February 1989

**Abstract.** The spectral distribution and integrated intensity of resonant Raman scattering was measured with tunable synchrotron radiation in the vicinity of the K edges of Cu and Zn and $L_{III}$ edge of Ho. The assumption of a constant density of final states is adequate to describe the cross section more than 5–10 eV below the absorption edges. Despite the poor energy resolution afforded by a solid state detector the lifetime width of the inner-shell hole was determined to within a fraction of an electron volt. In the case of the L shell especially, the sub-shell widths can be measured individually in a straightforward low-resolution experiment. The result of $4.8\pm0.2$ eV for the Ho $2p_{3/2}$ level is much closer to the predicted value of 4.0 eV than widths obtained from absorption edge spectroscopy.

## 1. Introduction

The theoretical prediction (Nozières and Abrahams 1974, Gavrila and Tugulea 1975) and the first experimental observation (Sparks 1974) of resonant Raman scattering (RRS) as a second-order scattering process in solids was soon followed by a few studies related both to theory and more accurate experiments. It was found that the gross features of RRS could be explained by the semiclassical scattering theory in dipole approximation (Eisenberger *et al* 1976, Bannett *et al* 1977, Suortti 1979), and the branching ratios seemed to follow those valid above the absorption edge, i.e. in fluorescence (Schaupp *et al* 1984, Manninen *et al* 1986). The differential cross section far below the absorption edge turned out to be well explained assuming a Lorentzian shape for the inner-shell hole (Schaupp *et al* 1984, Manninen *et al* 1985). Additionally a line-narrowing effect was observed at the absorption edge, i.e. the width of the emission line was less than the lifetime width (Eisenberger *et al* 1976). Since then the fine structure of the differential cross section of RRS, which depends on the crystal structure yielding information similar to XANES and EXAFS, has been studied. Basically the different role of the inner-shell hole in EXAFS and RRS processes can make RRS preferable in fine structure studies (Suortti *et al* 1987) although there are always at least two overlapping edges in RRS which makes the extraction of information more difficult.

The aim of the present study is twofold: we want to extend RRS studies to include an L-shell hole (all previous studies have been made at the K edge) and therefore a

0953-8984/89/345955+10$02.50  

measurement on the Ho $L_{III}$ edge was performed. We also want to use the measured cross sections to determine inner-shell energy widths, a method already tried in the 1930s (Richtmyer *et al* 1934, Beeman and Friedman 1939) with a semiclassical approach. We point out that this is a straightforward way to determine the total inner-shell energy widths (radiative + Auger) and therefore measurements on Cu and Zn samples were also made.

All the measurements were performed using tunable synchrotron radiation. The experimental cross sections were deduced from the measured data. Also theoretical RRS cross sections were calculated to check the validity of the approximations used to derive the energy widths.

## 2. Theory

In the following we consider an idealised experiment where a monochromatic incident beam is scattered by a thin sample. The various scattering processes are analysed with good energy and momentum resolution, and the transmitted beam is recorded at the same time. The attenuation of the beam is proportional to the integral of all scattering processes and therefore provides a sum rule for the scattering cross sections.

The theory of inelastic scattering including the resonant phenomena has been reviewed recently (Åberg and Tulkki 1985), with extensive reference to earlier work. These authors discuss in detail the K resonance under simplifying assumptions that restrict the final states to $(np_j)^{-1}$ and exclude all anisotropy effects. The differential cross section per unit frequency and solid angle for the K resonance scattering by $np_j$ electrons is given by

$$\frac{d^2\sigma}{d\omega_2\, d\Omega} = \frac{r_0^2}{2}\int_0^\infty \left(\frac{\omega_2}{\omega_1}\right)\left(\frac{(\Omega_{1s}-\Omega_{np_j})g_{np_j,1s}(\Omega_{1s}+\omega)\, dg_{1s}/d\omega}{(\Omega_{1s}+\omega-\omega_1)^2+\Gamma_{1s}^2/4\hbar^2}\right) \times \delta(\omega_1-\Omega_{np_j}-\omega-\omega_2)\, d\omega. \tag{1}$$

Here $\Omega_{1s}$ and $\Omega_{np_j}$ are the threshold frequencies, $g_{np_j,1s}$ the oscillator strength of the transition between the $(1s)^{-1}$ and $(np_j)^{-1}$ hole states, $\hbar\omega$ the kinetic energy of the ejected electron, $\hbar\omega_1$ the energy of the incident photon and $\hbar\omega_2$ that of the scattered photon. $\Gamma_{1s}$ is the width of the 1s level (FWHM), and $dg_{1s}/d\omega$ is the oscillator density, which is proportional to the density of empty states (DOS) and to the transition matrix element.

The final-state lifetimes can be included to lowest order by replacing the $\delta$ function in (1) by the normalised density function $dN_f/d\omega_2$ with the FWHM of $\Gamma_{np_j}$, where

$$\frac{dN_f}{d\omega_2} = \frac{\Gamma_{np_j}/2\pi\hbar}{(\omega_1-\Omega_{np_j}-\omega-\omega_2)^2+\Gamma_{np_j}^2/4\hbar^2}. \tag{2}$$

The cross section can be written in a more transparent form by using the condition $\omega_2+\omega=\omega_1-\Omega_{np_j}$ and writing $\Delta\Omega_{KL}=\Omega_{1s}-\Omega_{np_j}$ and $g_{LK}=g_{np_j,1s}$ for the scattering by $2p_j$ electrons ($j=\frac{1}{2},\frac{3}{2}$);

$$\frac{d^2\sigma}{d\omega_2\, d\Omega} = \frac{r_0^2}{2}\left(\frac{\omega_2}{\omega_1}\right)\frac{\Delta\Omega_{KL}g_{LK}(\Omega_{1s}+\omega)}{(\Delta\Omega_{KL}-\omega_2)^2+\Gamma_{1s}^2/4\hbar^2}\left(\frac{dg_{1s}}{d\omega}\right). \tag{3}$$

The cross section is essentially a Lorentzian centred at $\Delta\Omega_{KL}$ and modulated by $dg_{1s}/d\omega$. The contents of (3) are summarised graphically in figure 1, where a classical diagram of a scattering process is shown. The incident photon of energy $\hbar\omega_1$ excites an electron from the 1s state to continuum state of $\hbar\omega$. The hole at $-(\hbar\omega_1 - \hbar\omega)$ is filled from a $2p_j$ level, and a photon of the energy difference between the final and initial holes is emitted. The probability of this process is proportional to the K-level distribution at $-(\hbar\omega_1 - \hbar\omega)$ and to oscillator density $dg_{1s}/d\omega$.

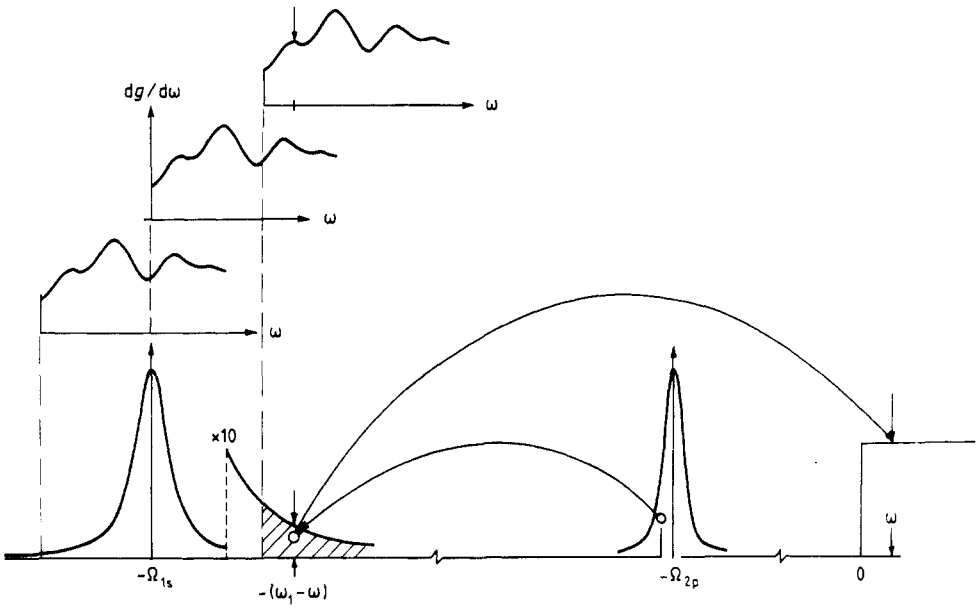


**Figure 1.** Schematic presentation of KL x-ray fluorescence and resonant Raman scattering (RRS). The K- and L-shell levels have Lorentzian distributions centred at $-\Omega_{1s}$ and $-\Omega_{2p}$, respectively. The energy of the incident x-rays is indicated by the edge of the oscillator density $dg/d\omega$ at $\omega = 0$. The total cross section is proportional to the product of the K-level distribution $dg/d\omega$ above this edge and three different cases are shown (from the bottom): fluorescence ($\omega_1 > \Omega_K$), transition to RRS ($\omega_1 = \Omega_K$) and RRS ($\omega_1 < \Omega_K$). The electron excitations are shown for RRS, and the 'active' part of the K level is indicated by hatching. The electron from the tail of the K level is excited to the continuum level $\omega$, and the hole is filled from the L-level. The energy of the scattered x-ray is $\hbar(\omega_1 - \omega - \Omega_L)$ and the intensity is proportional to the K-level distribution at $-(\omega_1 - \omega)$ and to $dg/d\omega$ at $\omega$.

The emission spectrum is the cross section (3) convoluted by the Lorentzian distributions of the $2p_j$ states, given by (2); a detailed formula has been worked out by Eisenberger *et al* (1976). Different types of information can be recovered from this spectrum according to the incident energy, as shown by the three cases studied below.

### 2.1. *Full fluorescence*, $\omega_1 - \Omega_{1s} > \Gamma_{1s}/\hbar$

In this case the whole Lorentzian distribution of the K-shell hole is 'active', and the spectrum of $\hbar\omega_2$ is this distribution convoluted by the Lorentzian of $(np_j)$ holes and modulated by the $dg_{1s}/d\omega$. Accordingly, fluorescence lines of widths $\Gamma_{1s} + \Gamma_{np_j}$ result. If the spread of the incident energy is much less than $\Gamma_{1s} + \Gamma_{np_j}$, the modulations due

to $dg_{1s}/d\omega$ are seen in the line shape. As $\omega_1$ is scanned the modulations move through the centre of the fluorescence line ($\omega_2 = \Delta\Omega_{KL}$) and even the total cross section, $d\sigma/d\Omega$, is substantially affected. The function $dg_{1s}/d\omega$, convoluted with a Lorentzian of the K-shell hole is obtained from the absorption coefficient or the intensity of fluorescence. The structures seen in either one are called XANES or EXAFS. The convolution by the K-shell distribution limits the resolution of the method where $dg_{1s}/d\omega$ is probed by the changes of the total cross section $d\sigma/d\Omega$.

### 2.2. *Transition to* RRS, $\omega_1 = \Omega_{1s}$

In this situation only the upper half of the K-shell distribution contributes. If $dg_{1s}/d\omega$ were a simple step function , the total cross section at $\omega_1 = \Omega_{1s}$ would be one half of that in full fluorescence. With a step function DOS the width of the fluorescence line is minimum, and is approximately equal to $\Gamma_{1s}/2 + \Gamma_{2p_j}$, when $\omega_1 = \Omega_{1s}$. This has been observed (Eisenberger *et al* 1976), and it can be used for very precise determination of the binding energy.

The situation is slightly more complicated with a realistic DOS, and the minimum linewidth occurs roughly where there is greatest fractional change in DOS across the Lorentzian, which may or may not correspond to the binding energy. The middle point of the steep rise of the absorption coefficient may deviate even more from $\omega_1 = \Omega_{1s}$.

### 2.3. RRS, $\Omega_{1s} - \omega_1 > \Gamma_{1s}/\hbar$

In this case only the upper tail of the Lorentzian distribution of the 1s state contributes. The spectrum of the scattered radiation, $\hbar\omega_2$, is the tail of this distribution, modulated by $dg_{1s}/d\omega$ and convoluted by the 2p distributions. This convolution makes the RRS spectrum a superposition of the components corresponding to the transitions from $2p_{1/2}$ and $2p_{3/2}$, which have an intensity ratio of 1:2. At sufficiently high atomic numbers these contributions are observed separately even with the solid state detector (Manninen *et al* 1985). The modulations due to $dg_{1s}/d\omega$ have been observed in in the RRS of Cu $K\alpha_1$ radiation from Ni using a focusing crystal spectrometer (Suortti *et al* 1987), although much of the modulations are damped by the superposition of the $1s2p_{1/2}$ and $1s2p_{3/2}$ spectra.

Sufficiently far below the threshold $dg_{1s}/d\omega$ can be replaced by the value that corresponds to the average energy of the ejected electron, $\hbar\bar{\omega}$, when the cross section is calculated. The leading term is then

$$\left(\frac{d\sigma}{d\Omega}\right)_{KL} = \frac{(\Omega_{1s} + \bar{\omega})}{4\pi^2\omega_1}\sigma_{1s}(\Omega_{1s} + \bar{\omega}) \tan^{-1}\left(\frac{\Gamma_{1s}/2}{\Delta E}\right) \tag{4}$$

where $\Delta E = \hbar\Omega_{1s} - \hbar\omega_1$ and $\sigma_{1s}(\Omega_{1s} + \bar{\omega})$ is the KL contribution to the photoelectric absorption. This functional form can be used for a determination of the zero point of $\Delta E$, i.e. the binding energy $\hbar\Omega_{1s}$, and the K-level width $\Gamma_{1s}$. The former is obtained from the requirement that a plot of $\omega_1(d\sigma/d\Omega)_{KL}$ against $\tan^{-1}(\Gamma/2\Delta E)$ is a straight line, and the latter from the slope of this line. This same idea was already used in the very early studies (Richtmyer *et al* 1934, Beeman and Friedman 1939), where $(d\sigma/d\Omega)_{KL}$ was deduced from the K-shell contribution to the absorption coefficient. The present determination is far more accurate, however, because the K-shell contribution is measured separately and not inferred from the total attenuation coefficient.

## 3. Experiment

All experiments included in this work were performed at the Daresbury storage ring. Because the desired energy range was below 10 keV and higher energies would only produce additional difficulties due to the harmonic energies passing through the monochromator, radiation from a bending magnet with a characteristic emission energy $E_c = 3.2$ keV was used instead of the wiggler which has $E_c = 14$ keV. The scattering geometry was similar to the previous work at LURE, Paris (Manninen *et al* 1986), i.e. the scattered radiation was measured at the scattering angle of 90° in the plane of the storage ring. Due to the polarisation factor this arrangement minimises the elastic and inelastic scattering arising from the $A^2$ term which would overlap the RRS spectrum.

Samples used in the experiment were polycrystalline foils. In each case incident energies from about 1 keV below the desired edge up to about 300 eV above the edge were used. The energy scale was checked a few times during each run by absorption edge scans. The accuracy of this procedure and its effect on the results is discussed later. The measuring time at each incident energy varied from 1 h far below the edge to 100 s above the edge. The scattered radiation was measured using a Si detector which had a resolution of 200 eV at 10 keV and a constant efficiency in the range of interest. The intensity of the monochromatic beam was monitored continuously using an ion chamber and these readings were used to correct the measured data for the beam decay. A Si(111) channel-cut monochromator having a resolution of about 1 eV was used. Contamination of the KL RRS in Cu and Zn and the $L_{III}M_{IV,V}$ RRS in Ho from fluorescence excited by the third monochromator harmonic was negligible but it did prevent the effective use of KM (Cu and Zn) and LN (Ho) contributions which totally overlapped with fluorescence produced by the harmonics.

This point is illustrated in figure 2 where there is a RRS spectrum of Cu taken at 8200 eV, i.e. 780 eV below Cu K edge. It is clearly seen that besides KL and KM contributions there is a significant Cu K$\alpha$ fluorescence and elastically scattered component overlapping with the KM RRS which should be only about 14 % compared with the KL RRS. Closer to the absorption edge these parasitic radiation components are relatively smaller due to the resonant behaviour of $\boldsymbol{p} \cdot \boldsymbol{A}$ term but no detailed analysis of the KM (or LN in Ho) component was performed. In the previous study (Manninen *et al* 1986) it was found that the branching ratio valid at the fluorescence was also true below the edge and therefore it was decided to use only the KL component in the present analysis. As can be seen in figure 2, it is well separated from the other scattering components.

Radiative cross sections were deduced from the measured count rates. In the symmetrical reflection geometry the energy dependence of the cross section is given by

$$\frac{d\sigma}{d\Omega} \propto \left(\frac{R}{IE_1^2}\right) \frac{\mu_{E_1} + \mu_{E_2}}{1 - \exp\left[-t\sqrt{2}(\mu_{E_1} + \mu_{E_2})\right]} \tag{5}$$

where $R$ is the count rate, $I$ the ion chamber current, $E_1^2$ comes from the ion chamber efficiency (Manninen *et al* 1986), $\mu_{E_1}$ and $\mu_{E_2}$ are the linear absorption coefficients for the incident and scattered beams and $t$ is the sample thickness.

Absorption coefficients for the incident beam were deduced by measuring the beam intensity with and without the sample using an ion chamber. The absolute values were obtained from reference values below and above the absorption edge (Saloman *et al*

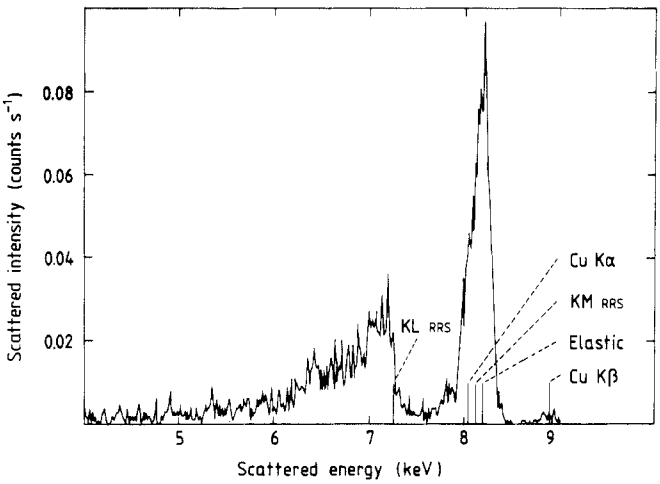


**Figure 2.** The experimental RRS spectrum of Cu, measured using 8200 eV radiation and scattering angle of 90°. Both elastic scattering due to the small nonlinear polarisation component and Cu K$\alpha$ fluorescence excited by harmonic wavelengths overlap with the KM RRS.

1988). Interpolated values from the same reference were used at the scattered radiation energy region since these values change only slowly with energy far from the absorption edges. For the dispersive RRS spectra the absorption coefficients corresponding to the maximum scattered energy could be used for the same reason. Near the edge, however, the absorption coefficients change very rapidly and small errors in the energy scale can greatly affect the calculations of the cross section, as seen in (5). This must be born in mind in the subsequent analysis of the data.

In order to produce absolute scattering cross sections, the data were normalised to the values from the literature at the energies above the XANES region, where small differences in energy calibration were not critical. The normalisation values were obtained by taking known absorption coefficients (Saloman *et al* 1988) , subtracting the small contributions from absorption by higher shells and scattering by a power-law fit, and multiplying by the known radiative yield (Bambynek *et al* 1972, Suortti 1971). This involves the assumption that the radiative yield stays constant in transition from fluorescence to RRS. The cross sections were then converted to more convenient electron units, i.e. given in terms of the Thomson cross section. Figure 3 shows the experimental cross sections for Cu, Zn and Ho given relative to the absorption edge (8071 eV for Ho $L_{III}$, 8979 eV for Cu K and 9659 for Zn K). Both XANES and near-EXAFS structures are seen as well as the contribution below the edge. The statistical accuracy is better than 0.5% and the main source of the experimental error in the cross sections was the uncertainty in the energy scale, except for energies far below the edge where statistical error dominates.

## 4. Results and discussion

According to the constant DOS model a plot of the cross section against $\tan^{-1}(\Gamma/2\Delta E)$ will, to a good approximation, give a straight line. Changes in the lifetime width $\Gamma$ will affect only the slope of the line far from the edge (see (4)) when $\Delta E \gg \Gamma$, while an

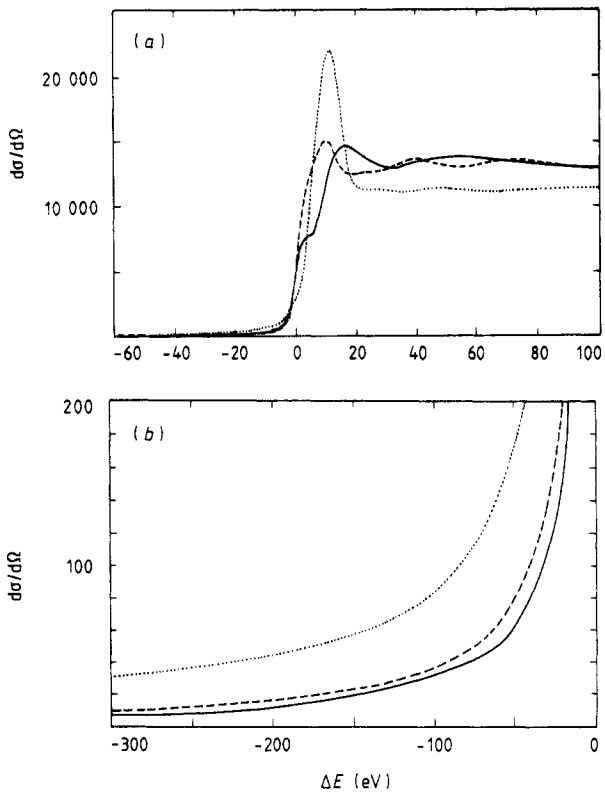


**Figure 3.** Experimental cross sections (given in electron units) of Cu (full curve), Zn (broken curve) and Ho (dotted curve) relative to the K (Cu and Zn) and $L_{III}$ absorption edges (*a*) around the absorption edge and (*b*) in the resonant Raman region.

incorrect choice of the energy scale will produce a curve. Futhermore, using (4) when $\omega_1 = \Omega_{1s} + \omega$ one can see that the slope of the line multiplied by $\pi$ gives the cross section for full fluorescence. Thus fitting the measured cross sections to this line gives, in principle, the possibility of determining both the lifetime width and energy scale.

The validity and sensitivity of the above procedure was established with a model calculation, where the cross section $d\sigma/d\Omega$ was calculated using a step function and in the case of Cu also using experimental data for the oscillator density $dg/d\omega$. The experimental $dg/d\omega$ was deduced from a high-resolution EXAFS measurement (Dartyge *et al* 1986) but the edge was cut in order to remove the effects of the instrumental broadening and the Lorentzian tail of the K-shell width below the edge. The differential cross section $d\sigma/d\Omega$ was first calculated using (3) for incident energies ranging from 500 eV below up to 500 eV above the K absorption edge and the total cross section $d\sigma/d\Omega$ was finally obtained by numerical integration.

An iterative arctan fit was then applied to the simulated data. The procedure described above gave back exactly the same $\Gamma$ and energy scale used in the model calculation. Precision in definition of $\Gamma$ turned out to be better than 0.1 eV with $\Gamma = 1.5$ eV and the energy scale could be determined with 0.2 eV accuracy in the case of the step function DOS. The use of the experimental oscillating DOS could be seen as deviations from the straight line only closer than 5–10 eV to the absorption edge. Thus the model calculation shows that the constant DOS model can be used with confidence

for the determination of $\Gamma$ and energy scale if points too close to the absorption edge are rejected.

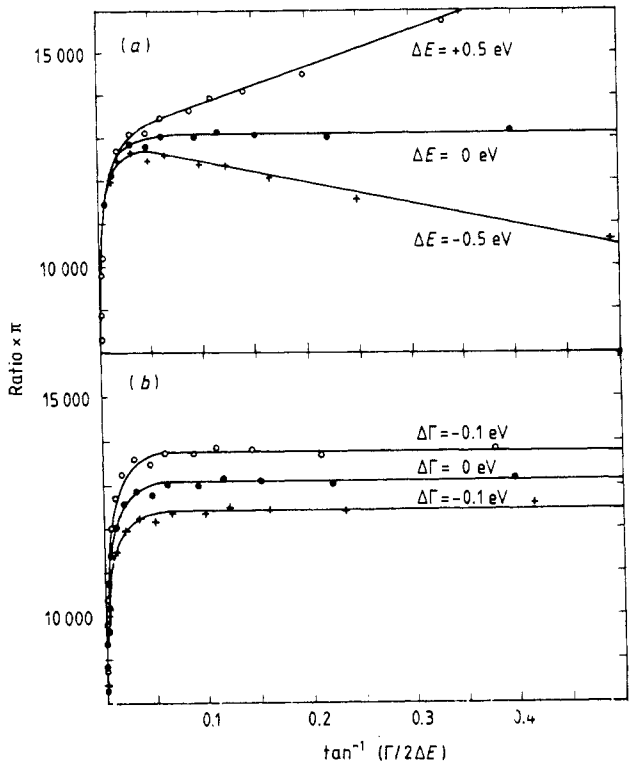


**Figure 4.** Experimental $\pi(d\sigma/d\Omega)/\tan^{-1}(\Gamma/2\Delta E)$ versus $\tan^{-1}(\Gamma/2\Delta E)$ for Zn. The constant DOS model predicts a horizontal line equal to the fluorescence cross section. The figure shows the sensitivity of the procedure when (*a*) the energy calibration is changed $\pm 0.5$ eV and (*b*) $\Gamma$ is changed $\pm 0.1$ eV from the best fit (middle line).

Using the model calculations as guidelines, $\Gamma_{1s}$ of Cu and Zn and $\Gamma_{2p_{3/2}}$ of Ho were determined. The sensitivity of this procedure is illustrated in figure 4 for the case of Zn. The optimum edge position is determined within $\pm 0.5$ eV and the uncertainty of $\Gamma_{1s}$ is about $\pm 0.1$ eV. It should be noticed that the uncertainty in $\Gamma_{1s}$ does not come from uncertainty in the normalisation of the cross section, i.e. absorption coefficient or fluorescence yield, but the uncertainty is due to the definition of the 'full fluorescence' level in the experimental data. This can been seen in figure 5 which shows the arctan plot of Zn including the whole energy range and the range used in the definition of $\Gamma$ and the energy scale. The result are summarised in table 1.

**Table 1.** Experimental lifetime widths

| | |
|---|---|
| Cu | $\Gamma_{1s} = 1.5 \pm 0.1$ eV |
| Zn | $\Gamma_{1s} = 1.9 \pm 0.1$ eV |
| Ho | $\Gamma_{2p_{3/2}} = 4.8 \pm 0.2$ eV |

These values can then be compared with those existing in the literature in order

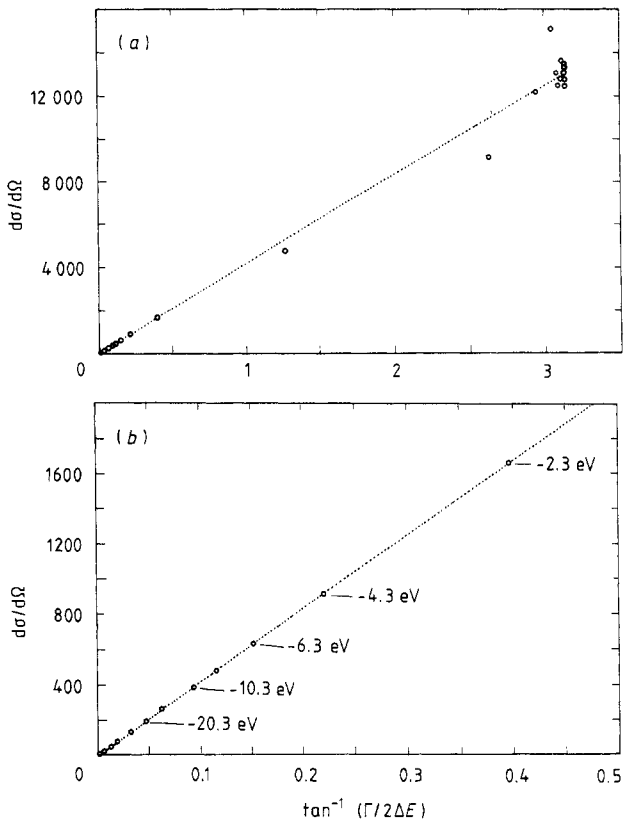


**Figure 5.** Experimental ($d\sigma/d\Omega$) versus $\tan^{-1}(\Gamma/2\Delta E)$ for Zn. (*a*) Oscillation above the edge makes the choice of the 'full-fluorescence' level difficult; this is the main source of error in the determination of $\Gamma$. (*b*) Expanded energy range below the edge. Some energies corresponding to the experimental values are indicated in the figure. The statistical error in the cross section is less than the size of the circle.

to estimate the potential use of the present method. First of all one should note that the experimental techniques used to measure inner-shell widths normally give either radiative or non-radiative widths, whereas in the present case the total $\Gamma$ is obtained. McGuire (1975) gives a summary based on available experimental and theoretical data on K- and L-shell widths. For Cu the experimental value is $\Gamma_{1s} = 1.5$ eV (Parratt 1959) and the theoretical value based on the interpolation of existing $\Gamma_{1s}$ calculations agrees with the measured one within the experimental accuracy. For Zn the same theory gives $\Gamma_{1s}$=1.78 eV; both values are very close to the present results. Kostroun *et al* (1971) have also calculated K-shell widths using different types of wavefunction and their results are slightly lower but the difference is smaller than the present experimental uncertainty.

Information on L-subshell widths is scarce and the few existing experimental values are widely scattered around the theoretical predictions. Additionally the problem is more complicated due to the importance of Coster–Kronig transitions especially in the case of $L_I$ and $L_{II}$ subshells. For Ho there are two calculations, McGuire (1971) and Walters and Bhalla (1971) which both give $\Gamma_{L_{III}} = 4.0$ eV. The experimental value of 10 eV obtained by Agarwal and Agarwal (1978) is apparently too large. On the other hand, the experimental value (Sevier 1972) of $\Gamma_{L_{III}}$=5.1 eV for Yb ($Z = 70$) is larger

than those predicted by the theories mentioned above. Our experimental result for Ho is closer to the theoretical values.

Finally if this method is compared with existing ones for measuring inner-shell energy widths it has several advantages: (i) it gives the total width, (ii) no high-resolution spectrometer is required, (iii) the result is not critically dependent on the model DOS and (iv) the desired component (for example KL) can be measured separately, which is much more accurate than the use of total absorption data. In the case of L subshells reliable results can be obtained with quite simple experimental apparatus.

## Acknowledgments

KH, SM and PS are indebted to the Finnish Academy and SC and MJC to the SERC for financial support. The help given by Dr G Clark during the course of measurements at Daresbury Laboratory is gratefully acknowledged.

## References

Åberg T and Tulkki J 1985 *Atomic Inner-Shell Physics* ed. B Crasemann (New York: Plenum) p 419
Agarwal B K and Agarwal B R K 1978 *J. Phys. C: Solid State Phys.* **11** 4223
Bambynek W, Crasemann B., Fink R W, Freund H U, Mark H, Swift C D, Price R E and Rao P V 1972 *Rev. Mod. Phys.* **44** 716
Bannett Y B, Rapaport D C and Freund J 1977 *Phys. Rev.* A **16** 2011
Beeman W and Friedman H 1939 *Phys. Rev.* **56** 392
Dartyge E, Depautex C, Dubuisson J M, Fontaine A, Jucha A, Leboucher P and Tourillon G 1986 *Nucl. Instrum. Meth.* A **246** 452
Eisenberger P, Platzman P M and Winick H 1976 *Phys. Rev.* B **13** 2377
Gavrila M and Tugulea M N 1975 *Rev. Roum. Phys.* **20** 209
Kostroun V O, Chen M H and Crasemann B 1971 *Phys. Rev.* A **3** 533
Manninen S, Alexandropoulos N G and Cooper M J 1985 *Phil. Mag.* B **52** 899
Manninen S, Suortti P, Cooper M J, Chomilier J and Loupias G 1986 *Phys. Rev.* B **34** 8351
McGuire J H 1971 *Phys. Rev.* A **3** 587
——1975 *Atomic Inner-Shell Physics* ed. B Crasemann (New York: Plenum) p 293
Nozières P and Abrahams E 1974 *Phys. Rev.* B **10** 3099
Parratt L G 1959 *Rev. Mod. Phys.* **31** 616
Richtmyer F K, Barnes S W and Ramberg E 1934 *Phys. Rev.* **46** 843
Saloman E B, Hubbell J H and Scofield J H 1988 *At. Data Nucl. Data Tables* **38** 1
Schaupp D, Czerwinski H, Smend F, Wenskus R, Schumacher A, Millhouse A M and Schenk-Strauss Z 1984 *Z. Phys.* A **319** 1
Scofield J H 1974 *At. Data Nucl. Data Tables* **14** 121
Sevier K D 1972 *Low Electron Spectrometry* (New York: Wiley)
Sparks C J 1974 *Phys. Rev. Lett.* **33** 262
Suortti P 1971 *J. Appl. Phys.* **42** 5821
——1979 *Phys. Status Solidi b* **91** 657
Suortti P, Eteläniemi V, Hämäläinen K and Manninen S 1987 *J. Physique Coll.* **48** C9 831
Walters D L and Bhalla C P 1971 *Phys. Rev.* A **3** 519